AN EXPERIMENTAL STUDY ON WIND WAVES AND LOW FREQUENCY OSICILLATIONS OF WATER SURFACE

Bandou, Toshiyuki
Department of Civil Engineering Hydraulics and Soil Mechanics, Kyushu University : Graduate student

Mitsuyasu, Hisashi
Reserch Institute for Applied Mechanics, Kyushu University : Professor

Kusaba, Tadao
Research Institute for applied Mechanics, Kyushu University : Research Institute for applied Mechanics, Kyushu University

https://doi.org/10.5109/6781036

出版情報：Reports of Research Institute for Applied Mechanics. 33 (101), pp.13-32, 1986-02. 九州大学応用力学研究所
バージョン：
権利関係：

Reports of Research Institute for Applied Mechanics
Vol. XXXIII, No. 101, 1986

AN EXPERIMENTAL STUDY ON WIND WAVES AND LOW FREQUENCY OSICILLATIONS OF WATER SURFACE

By Toshiyuki BANDOU*, Hisashi MITSUYASU† and Tadao KUSABA‡

The spectral form of wind-induced oscillations of water surface is investigated in a wind-wave tank for wide frequency range. The spectral form of wind waves is fitted to the JONSWAP spectrum, and spectral parameters α, γ, and σ are determined. The result shows that the present data satisfy approximately universal relations between the spectral parameters and the dimensionless fetch or the dimensionless frequency, which have been obtained from the wind and wave data in the ocean. In a low frequency region ($0.02f_m < f < 0.3f_m$, f_m : spectral peak frequency), an equilibrium spectrum is observed, which is represented approximately as $\Phi(f) = A \times f^{-0.5}$ (A is a parameter which increases with the diminsionless fetch). Many spikes are observed in the low frequency side of the spectrum measured near the upwind end of the tank, which are attributed to the longitudinal seiche and lateral seiche.

key words : Wind-wave spectrum, Wind-induced seiche

1. Introduction

When the wind blows over still water surface in a closed basin, the water oscillations with various time scales are generated. Well known oscillations are seiche, surf beat, wind waves, capillary waves, etc.

Great many experimental studies have been done for dominant part of the wind wave spectrum and various spectral forms have been proposed; PIERSON-MOSKOWITZ SPECTRUM[1] for fully developed wave spectrum and JONSWAP SPECTRUM[2] for fetch-limitted wave spectrum.

Recently, Mitsuyasu et al (1980)[3] determined empirical relations between the spectral parameters of the JONSWAP spectrum and the dimensionless fetch (or the dimensionless peak frequency) by using the ocean wave data. However,

* Graduate student, Department of Civil Engineering Hydraulics and Soil Mechanics, Kyushu University.
† Professor, Reserch Institute for Applied Mechanics, Kyushu University.
‡ Research Associate, Research Institute for applied Mechanics, Kyushu University.

it has not been clear whether or not such relations are satisfied for laboratory wave spectra.

In contrast to great many studies on the spectrum of wind waves, studies on the spectrum of wind-induced oscillations in a low frequency region are quite few. Therefore, the purpose of the present study is firstly to clarify the relations between the spectral parameters of wind waves and the demensionless fetch or the dimensionless peak frequency, and secondly to study the structure of the spectrum of low frequency oscillations generated by the wind.

For that purpose, we obtained the long records of stationary wind-generated oscillations of water surface to measure the power spectrum of wide frequency range with high frequency resolution and high degree of freedom. The measured power spectra are divided into two regions, low frequency region and dominant frequency region of wind waves, and spectral form in each frequency region is investigated in detail.

2. Experiment

2.1. Equipment and procedure

The experiment was carried out in a wind wave channel 0.8 m high, 0.6 m wide and with a usual test-section length of 14.58 m. Water depth in the channel was kept at 0.39 m.

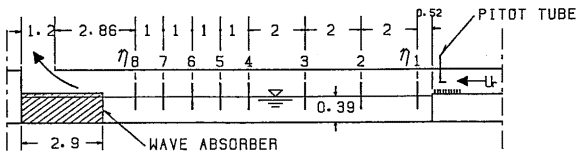

Fig. 1 Schematic diagram of wind wave channel (unit in m).

Figure 1 shows the arrangement of the equipment. Eight wave gauges (capacitance type) were installed at measuring stations No. 1, No. 2, ... , No. 8. The corresponding fetch of each station is as follows;

Station No.	1	2	3	4	5	6	7	8
Fetch(cm)	52	252	452	652	752	812	952	1,052

Wind speed U_r in the channel was changed in turn as U_r=5.0, 7.5, 10.0, 12.5, 15.0 (m/s). Here U_r is the wind speed measured with a Pitot static tube at 20 cm above the transition plate (see Fig. 1), and U_r corresponds approximately to a cross sectional mean speed in a test section. Waves were generated in the test section by wind of a prescribed speed. After the time when wind waves have attained a stationary state the surface elevation $\eta(t)$ was measured simultaneously at eight stations for 90 minutes for U_r=5.0, 7.5, 12.5, 15 m/s and

180 minutes for $U_r=10.0$ m/s. The data were recorded on a FM data recorder.

2.2. Analysis of wave data

Records of surface elevation $\eta(t)$ were digitized firstly at a sampling frequency of 200 Hz by using a high speed A-to-D converter. After applying a numerical filter of five line moving average to the data, the data were sampled at 40 Hz by skipping every five data. Finally the data is divided into subsamples, each of which contains 16384 data.

Frequency spectra of water surface fluctuations $\eta(t)$ were obtained through FFT method. After taking a sample mean of the spectra, triangular spectral filter was applied to them at each measuring points.

The conditions of the data analysis are summarized as follows:

Sampling frequency of the data; 40 Hz,

Nyquist frequency of the spectrum; 20 Hz,

Data length (per one sample); 409.5 sec,

Data point (per one sample); 16384,

Number of samples; 12 samples ($U_r=5.0$, 7.5, 12.5, 15.0 m/s) and 21 samples ($U_r=10.0$ m/s),

Spectral analysis; FFT method,

The lowest frequency; 2.44×10^{-3} Hz,

Elementary frequency bandwidth; 2.44×10^{-3} Hz,

Spectral filter; moving average of successive five line spectra ($f<1.0$ Hz), and thirty-one line spectra (1.0 Hz$<f<$20 Hz) with triangular filter.

Frequency resolution of the spectrum; 1.10×10^{-2} ($f<1.0$ Hz) and 5.86×10^{-2} (1.0 Hz$<f<$20 Hz),

Equivalent degrees of feedom; 108 ($f<1.0$ Hz) and 576 (1.0 Hz$<f<$20 Hz) for the data $U_r=5.0$, 7.5, 12.5, 15.0 m/s, 189 ($f<1.0$ Hz) and 1008 (1.0 Hz$<f<$20 Hz) for the data $U_r=10.0$ m/s.

2.3. Analysis of wind data

The wind profile over water surface was measured at each wave measuring stations by using a standard Pitot-tube and a Göttingen-type manometer. Almost every wind profiles near the water surface followed a logarithmic distribution;

$$U(z)=\frac{u_*}{\chi}\times\ln\frac{z}{z_o}\ , \tag{1}$$

where $U(z)$ is the wind velocity at an elevation z over the mean water level, u_* is the friction velicity of the wind, χ is the von Karman constant, and z_o is the roughness parameter. The friction velocity u_* and the roughness parameter z_o were determined by fitting the logarithmic profile (1) to the measured wind profiles near the water surface. The measured values of u_* and z_o are summarized in Table 1, where $\bar{u}_*$ is the mean values of the local friction velocities which were measured at the stations within a fetch.

Table 1 Wind Data

		5.0 m/s		7.5 m/s		10.0 m/s		12.5 m/s		15.0 m/s	
NO	F (cm)	U_M (cm/s)	$\overline{U_M}$ (cm/s)	U_M (cm/s)	$\overline{U_M}$ (cm/s)	U_M (cm/s)	$\overline{U_M}$ (cm/s)	U_M (cm/s)	$\overline{U_M}$ (cm/s)	U_M (cm/s)	$\overline{U_M}$ (cm/s)
1	52	8.0	8.0	22.0	22.0	28.5	28.5	37.5	37.5	67.0	67.0
2	252	22.0	15.0	38.0	30.0	54.5	41.5	67.0	52.2	111.0	89.0
3	452	23.0	17.7	47.5	35.8	66.0	49.7	80.0	61.5	141.0	106.3
4	652	24.0	19.2	49.5	39.2	66.5	53.9	83.0	66.9	162.5	120.4
5	752	24.5	20.3	50.0	41.4	67.0	56.5	83.5	70.2	171.0	130.5
6	852	25.0	21.1	50.0	42.8	67.0	58.3	84.0	72.5	178.0	138.4
7	952	25.0	21.6	50.0	43.8	67.0	59.5	84.0	74.1	181.5	144.6
8	1052	25.0	22.1	50.0	44.6	67.0	60.4	84.0	75.4	184.5	149.6

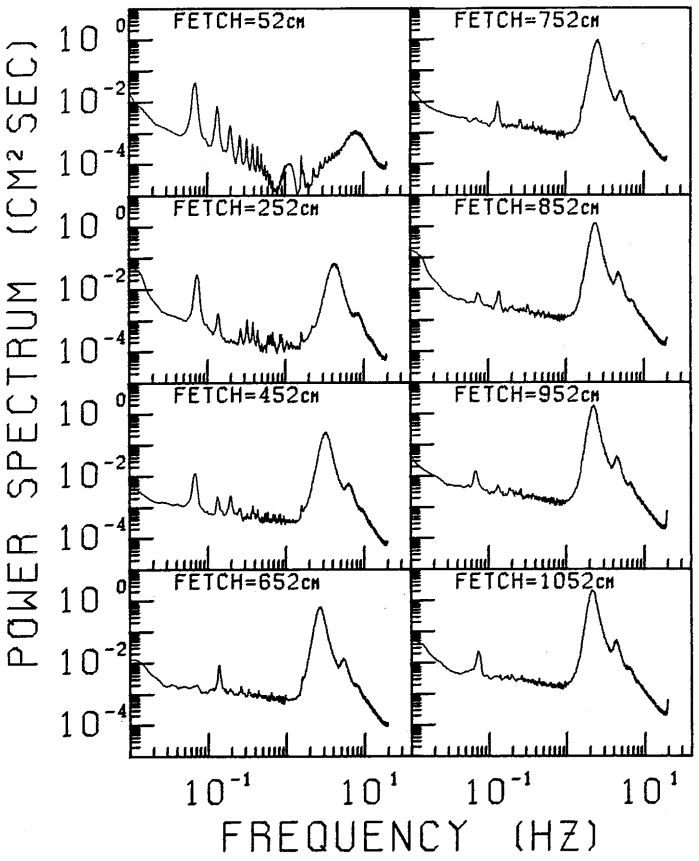

Fig. 2 Growth of the wave spectrum for wind speed $U_r = 10.0$ m/s.

3. Result

In the present study, we have used very long wave records for the spectral analysis. Thus the measured spectra extend to very low frequency range including dominant frequency range of wind waves, in addition to their high degree of freedom.

Figure 2 shows the evolution of the one-dimensional wave spectrum for the wind speed of $U_r=10.0$ m/s, when the fetch changes from 52 cm to 1,052 cm. In addition to usual spectral form of wind wave, the following characteristics can be seen clearly in the spectra.

(1) At short fetches, the spectra show many spikes of regular configuration.

(2) Some stationary spectral form can be seen at the low frequency region (10^{-2} Hz$\lesssim f\lesssim 10^{0}$ Hz) which is much lower than the region of wind waves.

Then the wave spectrum is divided into two regions as shown in Fig. 3; the low frequency region and the dominant frequency region of wind waves. Firstly the spectra in the region of wind waves are studied by fitting them to the JONSWAP spectrum. Particularly the relations between the spectral parameters and the dimensionless fetch (or the dimensionless peak frequency) are investigated. Secondly, the spectral form at the low frequency region is studied and related to the fetch and wind speed. Finally, the spike structure of the spectrum, which corresponds to the spectrum of seiche, is investigated.

3.1. The wind wave spectrum

In a previous study, the following fetch-dependent relations for the wind wave evergy E and for the spectral peak frequency f_m were derived (Mitsuyasu 1968)[4];

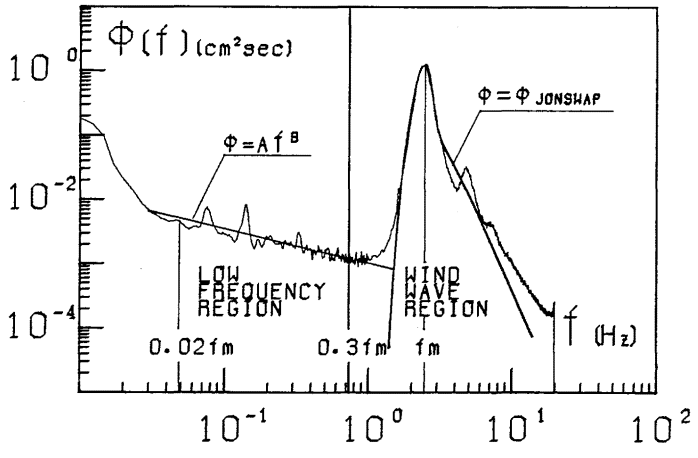

Fig. 3 Schematic representation of the spectral form of the low frequency region ($0.02f_m<f<0.3f_m$) and the wind wave region ($f>0.3f_m$); f_m is the spectral peak frequency.

$$\frac{g\sqrt{E}}{\bar{u}_*^{\,2}} = 1.31\times10^{-2}\times\left(\frac{gF}{\bar{u}_*^{\,2}}\right)^{0.504}, \tag{2}$$

$$\frac{\bar{u}_* f_m}{g} = 1.00\times\left(\frac{gF}{\bar{u}_*^{\,2}}\right)^{-0.330}. \tag{3}$$

Similar relations determined from the present data are

$$\frac{g\sqrt{E}}{\bar{u}_*^{\,2}} = 1.76\times10^{-2}\times\left(\frac{gF}{\bar{u}_*^{\,2}}\right)^{0.482}, \tag{4}$$

$$\frac{\bar{u}_* f_m}{g} = 0.653\times\left(\frac{gF}{\bar{u}_*^{\,2}}\right)^{-0.272}. \tag{5}$$

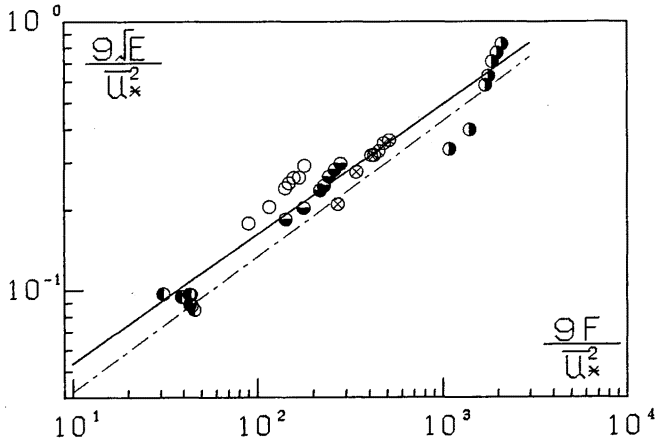

Fig. 4(a) Fetch relation for the wave energy E. Solid line is based on (4) and long dashed line is based on (2), Mitsuyasu (1968).

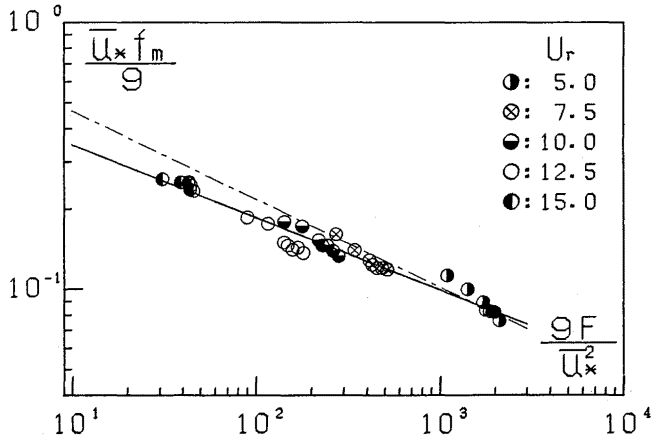

Fig. 4(b) Fetch relation for the spectral peak frequency f_m. Solid line is based on (5) and long dashed line is based on (3), Mitsuyasu (1968).

Although the present relations are different from the previous one, the diffrence are fairly small (see Figs. 4a and 4b).

For fetch-limited wind waves in the ocean, Hasselmann et al (1973) proposed the JONSWAP spectrum,

$$\Phi_{jsp}(f)=\frac{\alpha g^2}{(2\pi)^4}f^{-5}\exp\left(-\frac{5}{4}\left(\frac{f}{f_m}\right)^{-4}\right)\gamma^{\exp\left(-(f-f_m)^2/2\sigma^2 f_m^2\right)}, \tag{6}$$

$$\sigma=\begin{cases}\sigma_a & (f\leqq f_m)\\ \sigma_b & (f>f_m)\end{cases}, \tag{7}$$

where α and f_m are scale parameters, γ and σ are shape parameters, and γ is called as the "peak enhancement factor". In (7), σ_a and σ_b means the left and right side width of spectral peak (see Fig. 5).

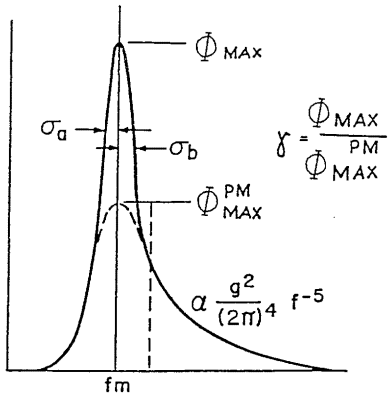

Fig. 5 Schematic representation of the JONSWAP spectrum (Hasselmann et al, 1973). Φ^{PM} is the Pierson-Moskowitz spectrum.

Recently Mitsuyasu et al (1980)[3] studied JONSWAP parameters α and γ for the ocean wave spectra, and proposed universal relations between these parameters and the dimensionless peak frequency $f_m U_{10}/g$ (or the dimensionless fetch gF/U_{10}^2), where U_{10} is the wind speed at the height 10 m.

In this section, we determined the parameters α, γ and σ by fitting the present wave spectra to the JONSWAP spectrum Φ_{jsp}. The results will be compared with those obtained from ocean wave data.

The value of α and γ are determined in the same way as in Hasselmann et al (1973);

$$\alpha=(0.65f_m)^{-1}\int_{1.35f_m}^{2f_m}(2\pi)^4 f^5 g^{-2}\exp\left(\frac{5}{4}\left(\frac{f}{f_m}\right)^{-4}\right)\Phi(f)\mathrm{d}f \tag{8}$$

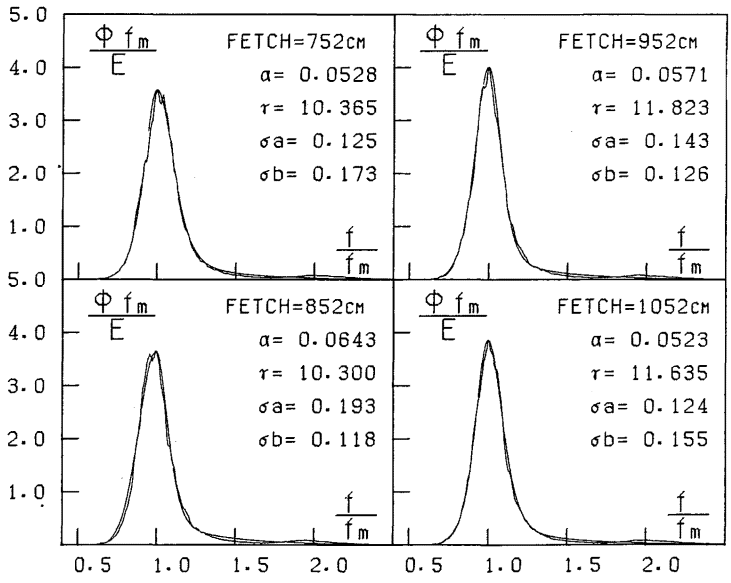

Fig. 6 Normalized form of the wave spectra for $U_r=10.0$ m/s. The smooth curve in each figure is the JONSWAP spectrum with the best-fit values of α, γ and σ.

$$\gamma = \Phi(f_m)(2\pi)^4 f_m{}^5 \exp\left(\frac{5}{4}\right)(\alpha g)^{-1} \tag{9}$$

σ_a and σ_b is determined as $\int_0^{f_m}|\Phi(f)-\Phi_{jsp}(f)|\mathrm{d}f$ is minimum and $\int_{f_m}^{\infty}|\Phi(f)-\Phi_{jsp}(f)|\mathrm{d}f$ is minimum, respectively.

Figure 6 shows a comparison of the wave spectra for $U_r=10.0$ m/s and $F=752$, 852, 952, 1,052 cm with the JONSWAP spectrum calculated in the above procedure. As can be seen from Fig. 6, the wave spectrum in a dominant frequency region can be fitted quite well to the JONSWAP spectrum by adjusting three parameters α, γ and σ.

In the laboratory scale, the peak frequency or fetch relations for parameter α and γ are given as follows (see Figs. 7 and 8),

$$\alpha = 0.282\times\left(\frac{\bar{u}_* f_m}{g}\right)^{0.848} = 1.84\times10^{-2}\times\left(\frac{U_{10} f_m}{g}\right)^{0.848} \tag{10}$$

$$\alpha = 0.217\times\left(\frac{gF}{\bar{u}_*{}^2}\right)^{-0.252} = 4.28\times10^{-2}\times\left(\frac{gF}{U_{10}^2}\right)^{-0.252} \tag{11}$$

$$\gamma = 1.82\times\left(\frac{\bar{u}_* f_m}{g}\right)^{-0.888} = 31.73\times\left(\frac{U_{10} f_m}{g}\right)^{-0.888} \tag{12}$$

$$\gamma = 2.43\times\left(\frac{gF}{\bar{u}_*{}^2}\right)^{0.261} = 13.04\times\left(\frac{gF}{U_{10}^2}\right)^{0.261} \tag{13}$$

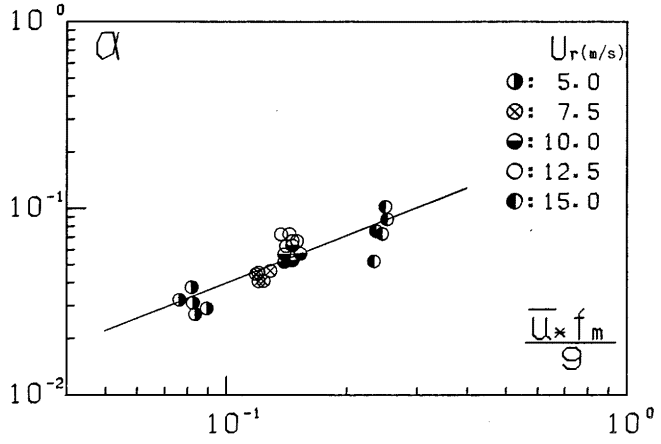

Fig. 7(a) The scale parameter α versus dimensionless peak frequency $\bar{u}_* f_m/g$.

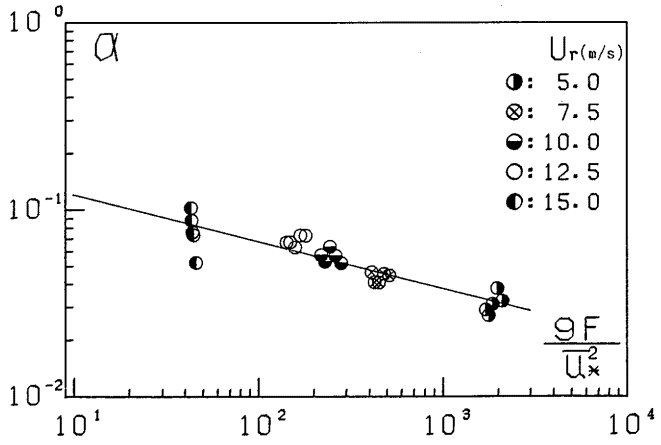

Fig. 7(b) The scale parameter α versus dimensionless fetch $gF/\bar{u}_*^2$.

where the friction velocity $\bar{u}_*$ is converted into the wind speed at the 10 m height U_{10} by

$$\bar{u}_*^2 = C_D \times U_{10}^2$$

and assuming the drag coefficient as $C_D = 1.6 \times 10^{-3}$.
The values of σ_a and σ_b in the present data is 0.1～0.2, and the dependence to the wind speed or fetch is not clear.

The mean value is

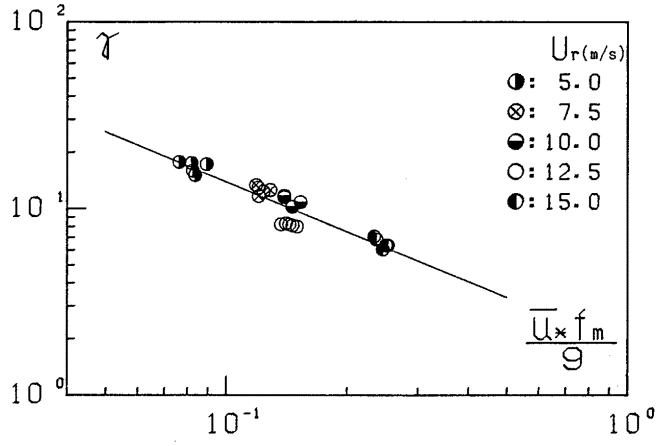

Fig. 8(a) The shape parameter γ versus dimensionless peak frequency $\bar{u}_* f_m/g$.

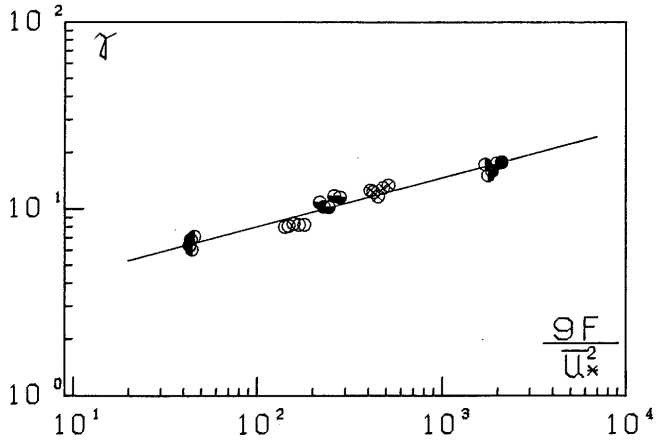

Fig. 8(b) The shape parameter γ versus dimensionless fetch $gF/\bar{u}_*^2$.

$$\bar{\sigma}_a = \bar{\sigma}_b \fallingdotseq 0.15 \ . \tag{14}$$

The present results are compared in Figs. 9 and 10 with those in the previous study (Mitsuyasu et al 1980). As shown in Figs. 9(a), 9(b), the values of α obtained in the present study are fairly close to the empirical relations determined from the ocean wave data (Mitsuyasu et al, 1980);

$$\alpha = 3.26\times10^{-2}\times\left(\frac{U_{10}f_m}{g}\right)^{\frac{2}{7}} , \tag{15}$$

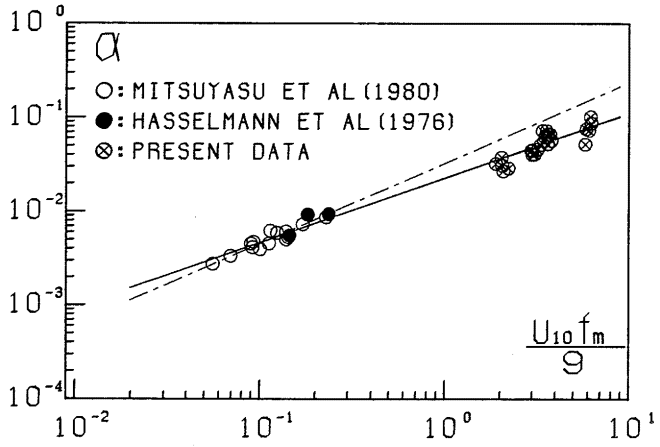

Fig. 9(a) The scale parameter α versus dimensionless peak frequency $U_{10}f_m/g$. Solid line is based on (17) and long dashed line is based on (15).

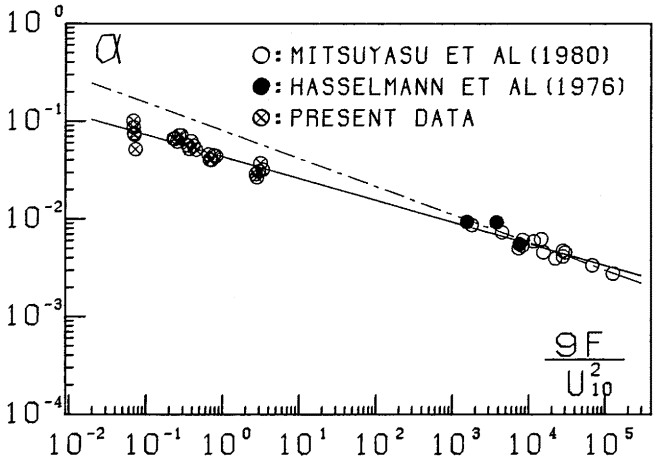

Fig. 9(b) The scale parameter α versus dimensionless fetch gF/U_{10}^2. Solid line based on Eq. (18) and long dashed line is based on (16).

$$\alpha = 8.17\times10^{-2}\times\left(\frac{gF}{U_{10}^2}\right)^{-\frac{2}{7}} . \tag{16}$$

though the present data are slightly smaller than those estimated from the previons relations. Revised relations obtained by using the present laboratory wave data and the previous ocean wave data are given by

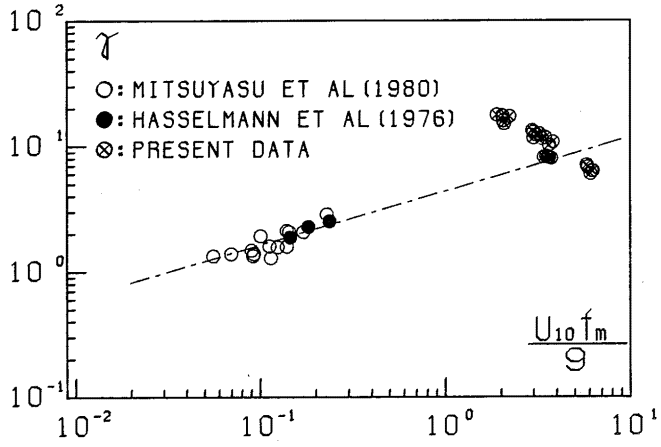

Fig. 10(a) The shape parameter γ versus dimensionless peak frequency $U_{10}f_m/g$. Long dashed line is based on Eq. (19).

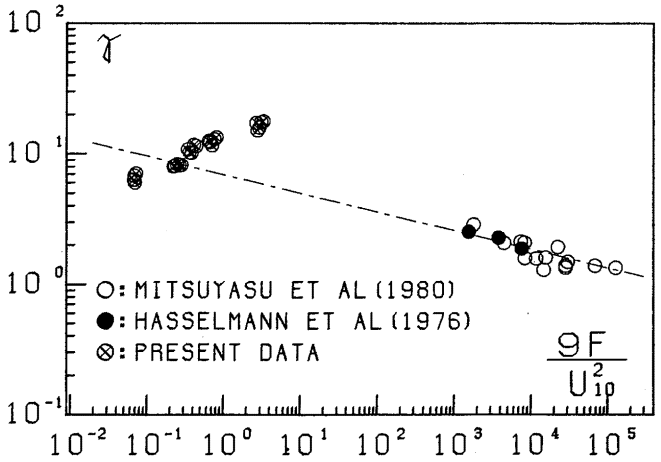

Fig. 10(b) The shape parameter γ versus dimensionless fetch gF/U_{10}^2. Long dashed line is based on Eq. (20).

$$\alpha = 2.27\times10^{-2}\times\left(\frac{U_{10}f_m}{g}\right)^{0.687}, \tag{17}$$

$$\alpha = 4.43\times10^{-2}\times\left(\frac{gF}{U_{10}^2}\right)^{-0.223}. \tag{18}$$

For the parameter γ, the result is complicated. In a rough sense, the present

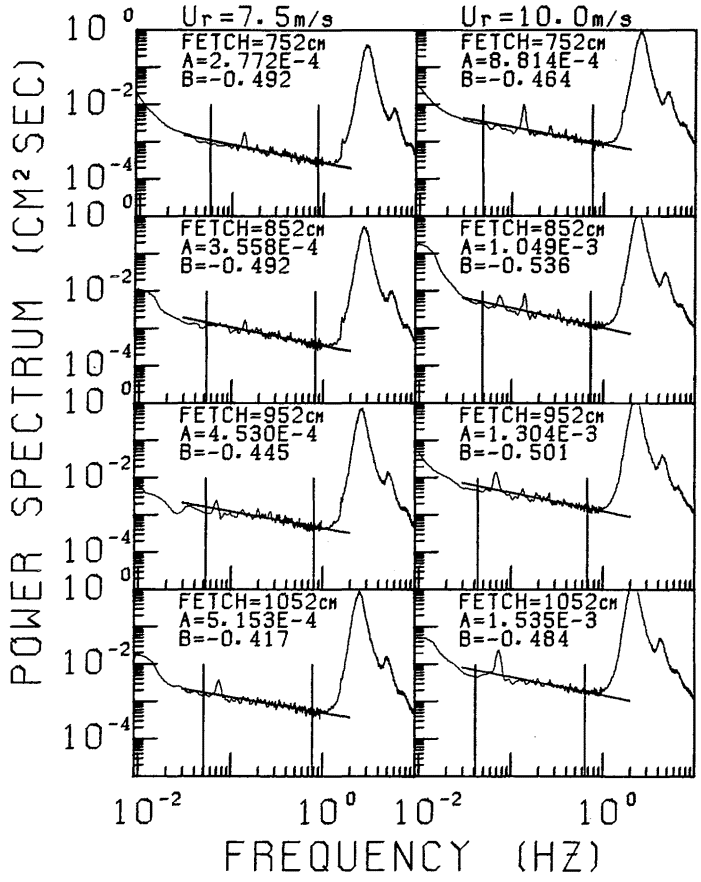

Fig. 11 The spectral form of low frequency region U_r=7.5, 10.0 m/s. Solid line is $\Phi(f)=A\times f^B$ with the best fit values of A and B in the region between two vertical line which represent $0.02f_m$ and $0.3f_m$.

data of γ is scatter around the previons relation determined from ocean wave data.

$$\gamma = 4.42\times\left(\frac{U_{10}f_m}{g}\right)^{\frac{3}{7}}, \tag{19}$$

$$\gamma = 7.0\times\left(\frac{gF}{U_{10}^2}\right)^{-\frac{1}{7}}. \tag{20}$$

However, different trend can be seen in the present data. That is, the parameter γ increases with decreasing Uf_m/g or with increasing gF/U^2, and γ follows to the empirical relations (12) and (13) as previously shown in Fig. 8. Such results

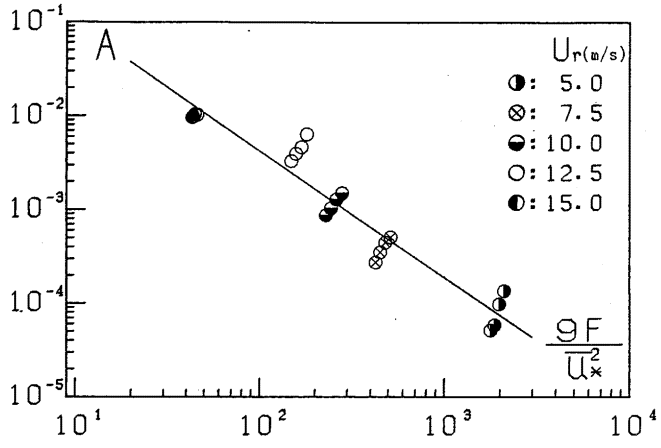

Fig. 12 Fetch relation for the parameter A.

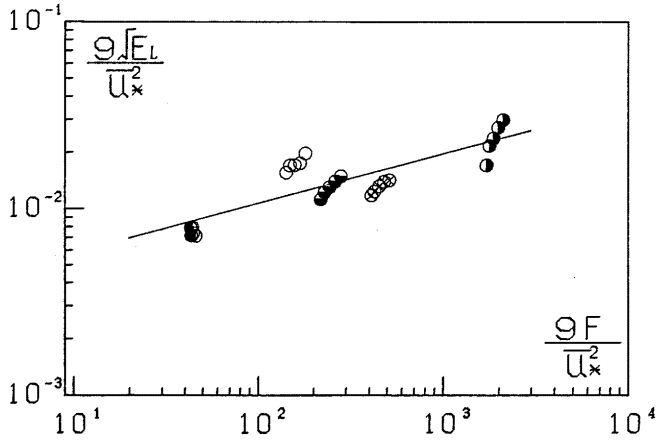

Fig. 13 Fetch relation for the wave energy E_l contained in the low frequency region, $0.02f_m<f<0.3f_m$.

for γ suggest that γ depends on another independent parameter (for example friction velocity u_*), but the relation is not clear in the present study.

The values of σ_a and σ_b are slightly larger than the values for ocean wave spectra, $\sigma_a=0.07$ $\sigma_b=0.09$. This is a rather unexpected result, because spectral energy of labolatory wind waves seems to be much concentrated than that of ocean waves.

3.2. The low frequency spectrum

Figure 11 shows a series of spectrum of the low frequency region. A kind of equilibrium form of the spectrum can be seen in a low frequency region of the spectra, $0.02f_m < f < 0.3f_m$.
The form can be expressed approximately as

$$\Phi(f) = A \times f^B \ , \tag{21}$$

as shown in Fig. 11 by a solid straight line.

The value of parameters A and B were determined by a least square method within the low frequency region, $f = 0.02f_m \sim 0.3f_m$.
As shown in Fig. 12, the parameter A is closely related to the dimensionless fetch $gF/\bar{u}_*^2$, and best fit relation is given by

$$A = 2.16 \times \left(\frac{gF}{\bar{u}_*^2}\right)^{-1.35} \ . \tag{22}$$

Parameter B seems to be related to wind speed and fetch, but this quantitive relation is not clear at this time. The value of B is approximately given by

$$B \fallingdotseq -0.5 \ . \tag{23}$$

Figure 13 shows a plot of spectral energy E_l in the low frequency region ($0.02f_m < f < 0.3f_m$) versus dimensionless fetch $gF/\bar{u}_*^2$.
The solid straight line

$$\frac{g\sqrt{E_l}}{\bar{u}_*^2} = 3.17 \times 10^{-3} \times \left(\frac{gF}{\bar{u}_*^2}\right)^{0.265} \ , \tag{24}$$

in Fig. 13 represents the best fit relation to the present data. Here the data of the short fetch is excluded because the spectral form is not clear owing to a lot of large spikes due to seiche.
As previously shown in 3.1, the relation between the dimensionless wave energy and the demensionless fetch is represented by (4).
Therefore, from (4) and (24) the ratio E_l/E is given by

$$\frac{E_l}{E} = 3.24 \times 10^{-3} \times \left(\frac{gF}{\bar{u}_*^2}\right)^{-0.434} \tag{25}$$

in the range of the dimensionless fetch ($gF/\bar{u}_*^2 = 10^1 \sim 10^3$).
The result means that the spectral energy contained in the low frequency region, $0.02f_m < f < 0.3f_m$, is at most 0.1 % of the total evergy of wind waves, and their ratio gradually decreases with increacing the dimensionless fetch.

3.3. The spectrum of seiche

Figure 14 shows the power spectrum of the surface elevation at the shortest fetch ($F = 52$ cm) for the wind speeds $U_r = 7.5$ m/s and 10.0 m/s. The solid and long dashed vertical lines correspond respectively to longitudinal (solid) and lateral (dashed) seiche of nth mode frequency f_{sn}, ($n = 1, 2, \ldots, 13$).
The frequency f_{sn} and the surface elevation ζ_n of nth mode seiche are given

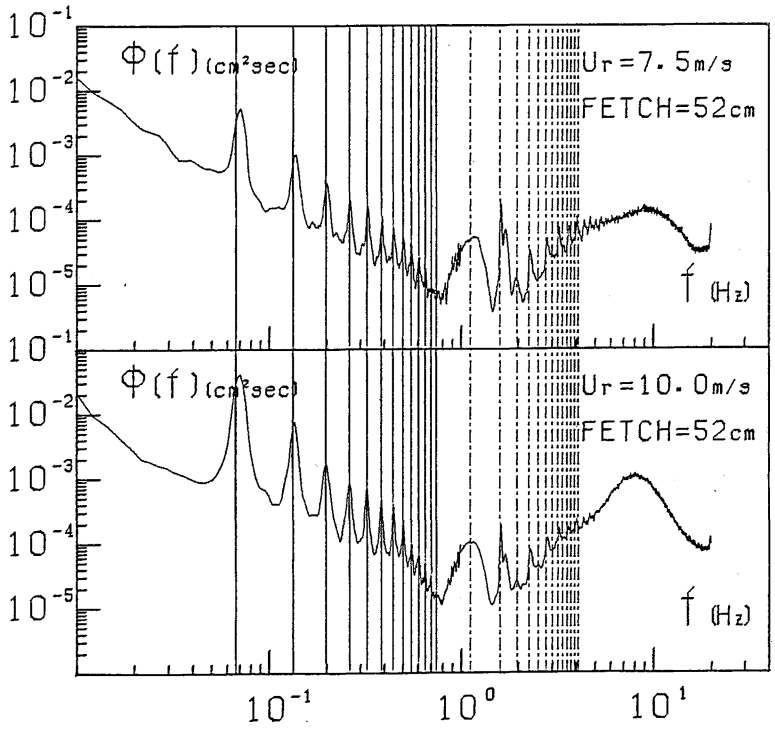

Fig. 14 The wave spectrum for U_r=7.5, 10 m/s. Solid lines and long dashed lines correspond to the longitudinal seiche (solid) and the lateral seiche (dashed) for nth mode frequency f_{sn}.

approximately by

$$\begin{cases} f_{sn} = \dfrac{nC}{2L} & C = \left(\dfrac{g}{k}\tanh kh\right)^{1/2} \\ \zeta_n = Ao\cos n\dfrac{\pi}{L}F_i & (i=1, 2, \ldots, 8) \end{cases} \tag{26}$$

where L is the test-section length 14.58 m for the longitudinal seiche, or the width of the channel 0.6 m for the lateral seiche, C is a wave velocity, Ao is a amplitude of seiche and F_i is a fetch of the measuring station number i.
Figure 14 shows that the spikes in the frequency rage $f \lesssim 1.0$ Hz represent the longitudinal seiche, and those in $f \gtrsim 1.0$ Hz represent lateral seiche. In Fig. 14, the lateral seiche of odd number mode are not clear, because the location of wave gauges are fairly close to the cross sectional center of the channel. Next we investigate the relation between energy of longitudinal seiche and the wind speed.

By taking the leakage effect in the spectral computation into account, energy of seiche is determined as

$$E'_{sn} = \int_{f_{sn-\delta}}^{f_{sn+\delta}} \Phi(f)\mathrm{d}f \qquad (\delta = 0.01\ \mathrm{Hz}) \ . \tag{27}$$

However, E'_{sn} thus obtained must be smaller than actual energy of seiche E_{sn} because measuring points in this experiment are slightly shifted from the seiche's loop. Thus the correction of the seiche's energy has been done as follows,

$$E_{sn} = E'_{sn}/COS^2 n\frac{\pi}{L}F_i \ . \tag{28}$$

The energy of seiche is calculated from the data obtained at the shortest fetch ($F_1 = 52$ cm), because the seiche spectrum at longer fetch is buried in the wind wave spectrum.

(i) The relation between the energy of fundamental mode of the seiche and wind speed.

Figure 15 shows the energy of primary mode of the longitudinal seiche E_{s1} versus mean friction velocity $\hat{u}_*$ for the wind speed $U_r = 7.5$, 10.0, 12.5, 15.0 m/s, where $\hat{u}_*$ is the mean value of the friction velocity at all measuring station, and the data of E_{s1} for $U_r = 5.0$ m/s is excluded because spike spectrum of primary

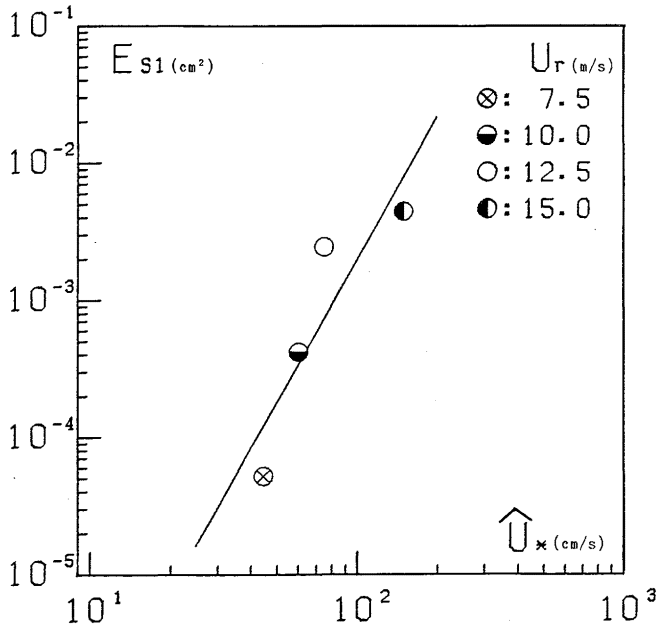

Fig. 15 Energy of fundamental mode of seiche versus friction velocity of wind.

mode is not clear (see Fig. 2).
Best fit relation for this data is given by

$$E_{s1} = 2.39 \times 10^{-10} \hat{u}_*^{3.46} \tag{29}$$

If we use the relation between E_{s1} and the wave height of primary mode of seiche H_{s1},

$$E_{s1} = \frac{1}{2} A o^2 = \frac{1}{8} H_{s1}^2 \ , \tag{30}$$

the equation (29) can be rewritten as

$$H_{s1} = 4.37 \times 10^{-5} \hat{u}_*^{1.73} \ . \tag{31}$$

For example, the value of H_{s1} for wind speed $U_r = 10.0$ m/s ($\hat{u}_* = 60.4$ cm) is 5.3×10^{-2} cm. On the other hand, the significant height of wind waves $H_{1/3}$ near the end of fetch, station No. 8 ($F_8 = 1{,}052$ cm), is 4.43 cm. Thus the ratio of H_{s1} to $H_{1/3}$ is the order of 10^{-2}. That is, the height of the wind-induced seiche is at most 1 % of significant wave height near the end of a fetch for $U_r = 10$ m/s.

On the other hand, wind setup η_τ generated by wind shear stress is given by

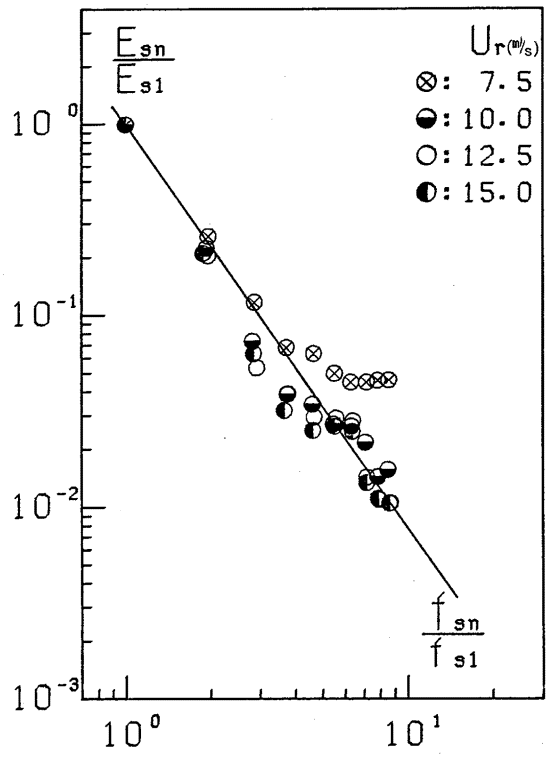

Fig. 16 Energy distribution in the modes of seiche.

$$\frac{\Delta\eta_\tau}{\Delta F}=1.01\times\frac{\rho_a\hat{u}_*^2}{\rho_w g h}\ , \tag{32}$$

(Mitsuyasu & Honda 1985)[5], where fetch, ρ_a is air density, ρ_w is water density and h is wave depth.

The ratio of H_{s1} to the wind setup $\Delta\eta_\tau$ between both sides of test-section for $U_r=10.0$ m/s is

$$\frac{H_{s1}}{\Delta\eta_\tau}\fallingdotseq 3.1\times10^{-1}$$

by using equation (31) and (32).

Therefore it is found that wave height of seiche's primary mode is roughly 30 % of wind setup. This fact suggest that we need to filter out the seiche when we measure the wind setup.

(ii) Energy of heigher modes of seiche.

Figure 16 shows the ratio E_{sn}/E_{s1} versus f_{sn}/f_{s1} ($n=2, 3, 4, \ldots$) for wind speeds $U_r=7.5$, 10.0, 12.5, 15.0 m/s.

Best fit relation is given by

$$\frac{E_{sn}}{E_{s1}}=\left(\frac{f_{sn}}{f_{s1}}\right)^{-2.1}\ . \tag{33}$$

The data for $U_r=7.5$ m/s shows a trend to deviate from the relation (33). This is partly due to the fact that the accuracy of the energy of seiche drops down with increasing mode number n or with decreasing wind speed U_r.

4. Conclusion

We measured very long records of wind-induced fluctuation of water surface in a stationary state to obtain the frequency spectrum of the surface fluctuation with high accuracy, high frequency resolution and wide frequency range extending to a very low frequency. By using the spectral data, we investigated the spectral form of the wind waves ($f\gtrsim1.0$ Hz) and that of low frequency fluctuation ($f\lesssim1.0$ Hz) in detail.

For the wind wave spectrum, the spectral form was fitted to the JONSWAP spectrum, and the spectral parameters α, γ, σ_a and σ_b are compared with the empirical relations obtained previously from ocean wave spectra.

For the low frequency spectrum, the equilibrium spectral form and the spike structure of the spectrum are investigated in detail.

The result is summarized as follows:

Spectral form of the wind wave region ($f\gtrsim1.0$ Hz); In a rough sense, the present data of α and γ follow to the fetch relations determined from the data of ocean wave spectra. However, if we closely examine the present laboratory data of α and γ, the fetch relation for α is slightly different from that obtained from the ocean wave, and that for γ shows a different fetch relation. The latter suggests that the parameter γ depends not only on the dimensionless fetch but also on

another parameter such as friction velocity u_*, though the definite relation had not been obtained yet. The values of σ_a and σ_b in the present data is 0.1～0.2, but their dependence on the dimensionless fetch is not clear at this time.

Spectral form of the low frequency region ($0.02f_m < f < 0.3f_m$); A kind of equilibrium form was found to exist in a low frequency region of the spectrum, $0.02f_m < f < 0.3f_m$, though the energy in this region is very small, say 0.1 % of the total energy of wind waves.

Spectral form of seiche; The many spikes in the spectrum are attributed to the longitudinal seiche ($f \lesssim 1.0$ Hz) and lateral seiche ($f \gtrsim 1.0$ Hz) in the wave tank. The wave height of the longitudinal seiche increases with the friction velocity of the wind, though its height is no more than 1 % of the significant wave height near the end of fetch, and approximately 20～30 % of the wind setup.

Acknowledgement

The authors are indebted to Mr. K. MARUBAYASHI and Mr. M. ISHIBASHI for their assistance in the laboratory experiment. They also wish to express their gratitudes to Dr. S. MIZUNO for his helpful discussions.

References

1) Pierson, W. J. and L. Moskowitz: *A proposed spectral form for fully developed wind seas based on the similarity theory of S. A. Kitaigorodskii.* J. Geophys. Res. 69, (1964), pp. 5181-5190.

2) Hasselmann, K., T. P. Barnett, E. Bouws, H. Carlson, D. E. Cartwright, K. Enke, J. A. Ewing, H. Gienapp, D. E. Hasselmann, P. Kruseman, A. Meerburg, P. Muller, D. E. Olbers, K. Richter, W. Swell and H. Walden. *Measurements of wind-wave growth and swell decay during the Joint North Sea Wave Project (JONSWAP).* Dtsch. Hydrogr. Z. 12, (1973), pp. 1-95.

3) Mitsuyasu, H., F. Tasai, T. Suhara, S. Mizuno, M. Ohkusu, T. Honda and K. Rikiishi. *Observation of the power spectrum of ocean waves using a cloverleaf buoy.* J. Phys. Oceanogr, Vol. 1, No. 2, (1980), pp. 286-296.

4) Mitsuyasu, H.: *On the growth of the spectrum of wind-generated waves (I).* Rep. Res. Inst. Appl. Mech., Kyushu Univ., Vol. 16, (1968), pp. 459-482.

5) Mitsuyasu, H. and T. Honda: *The effects of surfactant on certain air-sea interaction phenomena.* Proc. IUCRM Symposium of Wave Dynamics and Radio Probing of Ocean Surface, (1985).

(Received November 29, 1985)